

Raman spectroscopy of Fermi polarons

Hui Hu¹ and Xia-Ji Liu¹

¹Centre for Quantum Technology Theory, Swinburne University of Technology, Melbourne, Victoria 3122, Australia

(Dated: December 2, 2022)

By using a non-self-consistent many-body T -matrix theory, we calculate the finite-temperature Raman spectroscopy of a mobile impurity immersed in a Fermi bath in three dimensions. The dependences of the Raman spectrum on the transferred momentum, temperature, and impurity-bath interaction are discussed in detail. We confirm that the peak in the Raman spectrum shows a weaker dependence on the impurity concentration than that in the radio-frequency spectroscopy, due to the nonzero transferred momentum, as anticipated. We compare our theoretical prediction with the recent measurement by Gal Ness *et al.* in Physical Review X **10**, 041019 (2020) without any adjustable parameters. At weak coupling, we find a good quantitative agreement. However, close to the Feshbach resonance the agreement becomes worse. At strong coupling, we find that an unrealistic Fermi bath temperature might be needed, in order to account for the experimental data.

I. INTRODUCTION

Fermi polarons - quasiparticles formed when impurities move inside a Fermi bath - have received increasing attentions from researchers in different research fields, due to the rapid experimental advances in ultracold atomic physics. Nowadays, Fermi polarons can be routinely realized by using a highly imbalanced two-component Fermi-Fermi mixture [1–4], where the minority atoms play the role of impurities. The interaction between the impurity and the majority Fermi bath or Fermi sea can be tuned precisely with the help of Feshbach resonances [5]. Many useful techniques have been developed to characterize the quasiparticle properties of Fermi polarons, such as the radio-frequency spectroscopy [6–11], Ramsey interferometry [12], Rabi oscillation [8, 10], and Raman spectroscopy [13]. As a result, a number of intriguing features of Fermi polarons have been revealed [14, 15], including the excited branch of repulsive polarons [8–10, 16], and the disappearance of attractive polarons at sufficiently large impurity-bath coupling [13, 17–19].

Here, we are interested in the Raman spectroscopy, which has been applied most recently by Gal Ness and co-workers to observe the polaron-molecule transition [13]. In this experiment, the Fermi bath temperature is about one-fifth Fermi temperature (i.e., $0.2T_F$), and the trap-average impurity concentration, defined by $x = n_{\text{imp}}/n$ with n_{imp} (n) being the density of impurity and (bath) atoms, is about 0.23. To account for the temperature effect, the experimental data have been analyzed by using a *phenomenological* theory, where the system is treated as a non-interacting thermal mixture of polarons and molecules [13]. The thermal distributions or numbers of polarons and molecules are determined respectively according to their zero-temperature energy, calculated using the variational Chevy ansatz at the lowest level of particle-hole excitations [20]. A set of free fitting parameters, such as the polaron residue \mathcal{Z} , polaron temperature T_P (which might be different from the Fermi bath temperature) and effective binding energy of molecules, have been introduced to fit the data and to extract the polaron energy and molecule binding energy [13].

In this work, we would like to theoretically understand the measured Raman spectrum, based on a finite-temperature *microscopic* theory within the non-self-consistent many-body T -matrix approximation [21, 22]. At zero temperature, the non-self-consistent T -matrix approximation is fully equivalent to the variational Chevy ansatz with one-particle-hole excitation [23]. The finite-temperature extension of the T -matrix theory [21, 24, 25] allows us to improve the phenomenological treatment used in the experimental analysis, at least in the weak coupling regime, where attractive polarons are well-defined quasiparticles in the ground state [18, 23].

Indeed, for weak coupling we find that our theory agrees very well with the experimental data, without any free adjustable parameters. In the vicinity of the Feshbach resonance of the impurity-bath interaction, however, the experimental data appear to lie systematically lower than the theoretical prediction. To theoretically account for the data, we need to significantly increase the Fermi bath temperature. This is somehow consistent with the experimental observation that the extracted polaron temperature T_P is systematically higher than the Fermi bath temperature near the Feshbach resonance. Finally, for the strong coupling case our theory fails to explain the experimental data with any reasonable Fermi bath temperature. This failure clearly indicates the importance of developing a better description of Fermi polarons near the polaron-molecule transition, by extending more reliable zero-temperature theories such as the functional renormalization group [26] and diagrammatic Monte Carlo simulation [17, 27] to the finite-temperature case.

The rest of the paper is organized as follows. In the next section (Sec. II), we briefly review the non-self-consistent many-body T -matrix theory for Fermi polarons at finite temperature. In Sec. III, we first discuss in detail the properties of Raman spectroscopy in the ejection scheme and investigate the spectrum as functions of the transferred momentum, impurity concentration, temperature, and the impurity-bath interaction strength. We then compare our theoretical predictions with the ex-

perimental data. We also briefly consider the injection Raman spectrum. Finally, Sec. IV is devoted to the conclusions and outlooks. In Appendix A, we also consider the effect of spatial inhomogeneity on the Raman spectrum, caused by the external harmonic traps.

II. THE NON-SELF-CONSISTENT MANY-BODY T -MATRIX THEORY

The non-self-consistent many-body T -matrix theory of Fermi polarons at finite temperature has been discussed at length in Ref. [21]. Here, for self-containedness we briefly review the key equations in the following. The Fermi polaron system under consideration involves an impurity of mass m_I interacting with a homogeneous bath of fermionic atoms of mass m . It can be described by a model Hamiltonian,

$$\mathcal{H} = \sum_{\mathbf{k}} \epsilon_{\mathbf{k}} c_{\mathbf{k}}^{\dagger} c_{\mathbf{k}} + \sum_{\mathbf{p}} \epsilon_{\mathbf{p}}^{(I)} d_{\mathbf{p}}^{\dagger} d_{\mathbf{p}} + \frac{g}{V} \sum_{\mathbf{k}\mathbf{p}\mathbf{q}} c_{\mathbf{k}}^{\dagger} d_{\mathbf{q}-\mathbf{k}}^{\dagger} d_{\mathbf{q}-\mathbf{p}} c_{\mathbf{p}}, \quad (1)$$

where $c_{\mathbf{k}}^{\dagger}$ ($d_{\mathbf{p}}^{\dagger}$) are the creation field operators for fermionic atoms (impurity) with momentum \mathbf{k} (\mathbf{p}) and single-particle dispersion relation $\epsilon_{\mathbf{k}} = \hbar^2 \mathbf{k}^2 / (2m)$ ($\epsilon_{\mathbf{p}}^{(I)} = \hbar^2 \mathbf{p}^2 / (2m_I)$), and V is the system volume. The last term in the Hamiltonian describes the s -wave contact interaction between impurity and bath with a bare coupling strength g , which is to be regularized via the relation,

$$\frac{1}{g} = \frac{m_r}{2\pi\hbar^2 a} - \frac{1}{V} \sum_{\mathbf{p}} \frac{2m_r}{\hbar^2 \mathbf{p}^2}. \quad (2)$$

Here, a is the s -wave scattering length between impurity and the Fermi bath, $m_r \equiv mm_I / (m + m_I)$ is the reduced mass for the impurity-bath scattering. Throughout the work, we always take $m_I = m$, so $m_r = m/2$. The number of fermionic atoms in the Fermi bath (n) can be tuned by adjusting the chemical potential $\mu(T)$ at nonzero temperature T . We often measure the single-particle energy of the bath from the chemical potential and therefore define $\xi_{\mathbf{k}} \equiv \epsilon_{\mathbf{k}} - \mu$.

To solve the Fermi polaron problem, the key quantity of interest is the (retarded) impurity Green function,

$$G_R(\mathbf{k}, \omega) = \frac{1}{\omega - \epsilon_{\mathbf{k}}^{(I)} - \Sigma_R(\mathbf{k}, \omega)}, \quad (3)$$

and its associated single-particle spectral function, $A(\mathbf{k}, \omega) \equiv -(1/\pi) \text{Im} G_R(\mathbf{k}, \omega)$. In the single-impurity limit, within the non-self-consistent many-body T -matrix theory [21], the (retarded) self-energy $\Sigma_R(\mathbf{k}, \omega)$ can be calculated by summing all the ladder-type diagrams, which gives rise to an expression,

$$\Sigma_R(\mathbf{k}, \omega) = \frac{1}{V} \sum_{\mathbf{q}} f(\xi_{\mathbf{q}-\mathbf{k}}) \Gamma_R(\mathbf{q}, \omega + \xi_{\mathbf{q}-\mathbf{k}}), \quad (4)$$

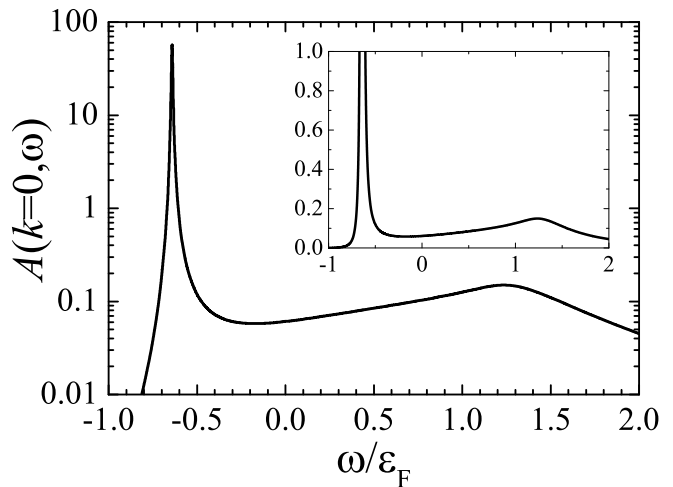


FIG. 1. The zero-momentum impurity spectral function $A(\mathbf{k} = 0, \omega)$ in the unitary limit $1/a = 0$. The spectral function is in units of ϵ_F^{-1} , where $\epsilon_F \equiv \hbar^2 k_F^2 / (2m)$ and $k_F = (6\pi^2 n)^{1/3}$ are the Fermi energy and Fermi wavevector, respectively. The temperature is $T = 0.2T_F = 0.2\epsilon_F / k_B$. The inset shows the spectral function in the linear scale.

where $f(x) \equiv 1/(e^{\beta x} + 1)$ with $\beta \equiv 1/(k_B T)$ being the Fermi-Dirac distribution function, and $\Gamma_R(\mathbf{q}, \Omega)$ is the vertex function, whose inverse is given by $(\Omega^+ \equiv \Omega + i0^+)$,

$$\chi_R(\mathbf{q}, \Omega) \equiv \Gamma_R^{-1}(\mathbf{q}, \Omega) = \chi_R^{(2b)} + \chi_R^{(mb)}, \quad (5)$$

$$\chi_R^{(2b)} = \frac{m_r}{2\pi\hbar^2 a} - \frac{1}{V} \sum_{\mathbf{k}} \left[\frac{1}{\Omega^+ - \xi_{\mathbf{k}} - \epsilon_{\mathbf{q}-\mathbf{k}}^{(I)}} + \frac{2m_r}{\hbar^2 \mathbf{k}^2} \right],$$

$$\chi_R^{(mb)} = \frac{1}{V} \sum_{\mathbf{k}} \frac{f(\xi_{\mathbf{k}})}{\Omega^+ - \xi_{\mathbf{k}} - \epsilon_{\mathbf{q}-\mathbf{k}}^{(I)}}.$$

As discussed in Ref. [21], the two-dimensional integrals in the calculations of the inverse vertex function $\Gamma_R^{-1}(\mathbf{q}, \Omega)$ can be efficiently evaluated, leading to fast and accurate determination of the (retarded) self-energy $\Sigma_R(\mathbf{k}, \omega)$ and consequently the single-particle spectral function $A(\mathbf{k}, \omega)$.

As an example, in Fig. 1 we show the zero-momentum impurity spectral function $A(\mathbf{k} = 0, \omega)$ at the Feshbach resonance, where the s -wave scattering length a between the impurity and Fermi bath diverges. A finite temperature typically leads to a nonzero thermal decay of the attractive Fermi polaron, as given by $\Gamma = -2\mathcal{Z} \text{Im} \Sigma_R(\mathbf{0}, \mathcal{E}_P)$, where \mathcal{E}_P is the polaron energy and $\mathcal{Z} = [1 - \partial \text{Re} \Sigma_R(\mathbf{0}, \omega) / \partial \omega]_{\omega=\mathcal{E}_P}^{-1}$ is the residue of the attractive polaron. At the low temperature considered in Fig. 1 (i.e., $T = 0.2T_F$), the decay rate $\Gamma \simeq 0.008\epsilon_F$ is very small, as indicated by the narrow full width at half maximum (FWHM) of the spectral function. This leads to a sharp peak at the polaron energy $\mathcal{E}_P \simeq -0.64\epsilon_F$. There is also a broad peak at much higher energy $\sim \epsilon_F$, which may be understood as a precursor of the repulsive polaron. Our accurate determination of the impurity spectral function is able to capture both sharply peaked

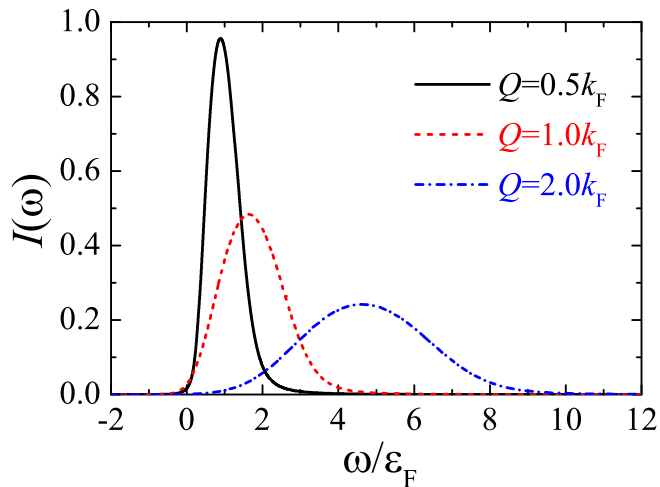


FIG. 2. The ejection Raman spectrum in the unitary limit and $T = 0.2T_F$, at different transferred momenta as indicated. The spectra are in units of ε_F^{-1} , and are normalized to unity (i.e., $\int d\omega I(\omega) = 1$). This can be achieved by dividing $I(\omega)$ the impurity density n_{imp} . We have taken an impurity concentration $n_{\text{imp}} = 0.15n$.

attractive polaron and broadly distributed repulsive polaron, allowing us to perform a microscopic calculation of the Raman spectrum at finite temperature, as we shall discuss in detail as follows.

III. RESULTS AND DISCUSSIONS

A. Ejection Raman spectroscopy

In the Raman spectroscopy experiment [13], initially the impurity is in the interacting state with the Fermi bath. It is then transferred to a non-interacting state using Raman beams with the energy ω and momentum \mathbf{Q} . In this *ejection* scheme, according to the linear response theory the transfer rate is proportional to [13, 28, 29],

$$I(\omega) = \frac{1}{V} \sum_{\mathbf{k}} A \left[\mathbf{k}, \epsilon_{\mathbf{k}+\mathbf{Q}}^{(I)} - \omega \right] f \left(\epsilon_{\mathbf{k}+\mathbf{Q}}^{(I)} - \omega - \mu_I \right). \quad (6)$$

Here, we have assumed a fermionic impurity according to the experiment [13]. To account for the finite impurity density n_{imp} , we have also introduced an impurity chemical potential μ_I , which is to be determined by the number equation,

$$n_{\text{imp}} = \frac{1}{V} \sum_{\mathbf{k}} \int_{-\infty}^{+\infty} d\omega f(\omega - \mu_I) A(\mathbf{k}, \omega). \quad (7)$$

It is readily seen that the ejection Raman spectrum is normalized to the impurity density, i.e., $\int d\omega I(\omega) = n_{\text{imp}}$. Moreover, in the limit of zero transferred momentum $Q = 0$, the Raman spectroscopy simply recovers the

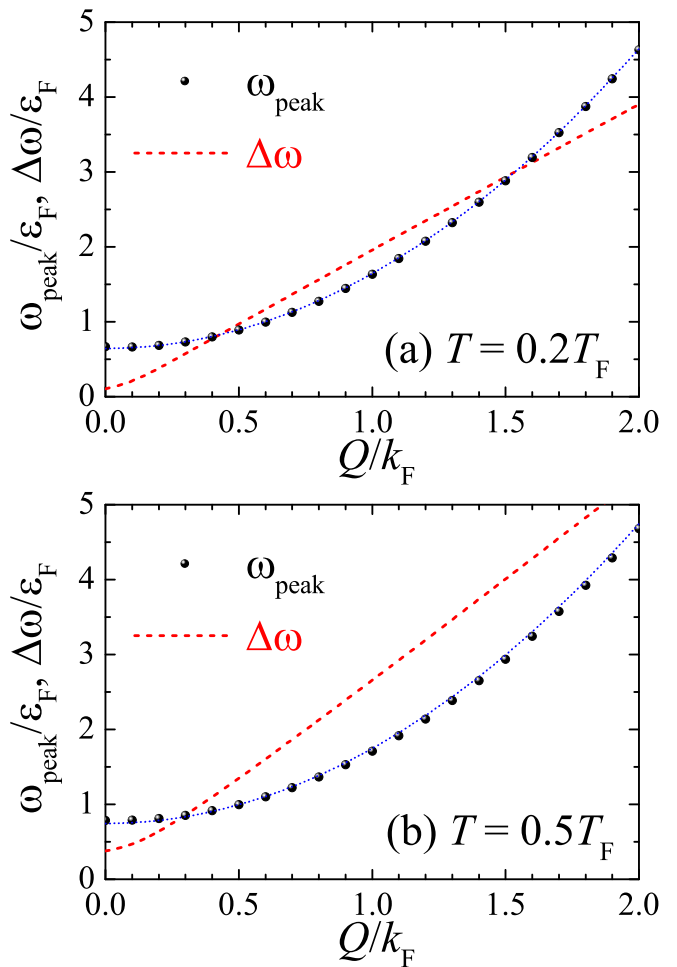


FIG. 3. The position and width of the peak in the ejection Raman spectrum as a function of the transferred momentum Q , at $T = 0.2T_F$ (a) and $T = 0.5T_F$ (b). Here, we consider the unitary limit with $1/(k_F a) = 0$. The blue dashed line in each plot shows the anticipated peak position $\omega_{\text{peak}} = \hbar^2 Q^2 / (2m) - \varepsilon_P$. The impurity concentration is $n_{\text{imp}}/n = 0.15$.

well-studied radio-frequency spectroscopy [6, 11, 21]. In Fig. 2, we report exemplified Raman spectra at different transferred Raman momenta for the unitary impurity-bath interaction. As the momentum Q increases, the Raman peak becomes broader and quickly shifts to high energy.

The blue shift of the peak with transferred momentum can be easily understood from the coherent part of the polaron spectral function, which at zero temperature takes the form [13],

$$A_{\text{coh}}(\mathbf{k}, \omega) \simeq \mathcal{Z} \delta \left[\omega - \left(\varepsilon_P + \frac{\hbar^2 k^2}{2m^*} \right) \right], \quad (8)$$

where the polaron mass m^* is close to the mass of bare atoms, $m^* \simeq m_I = m$, unless near the polaron-molecule transition. By substituting A_{coh} into the ejection expression Eq. (6), we find a coherent contribution to the

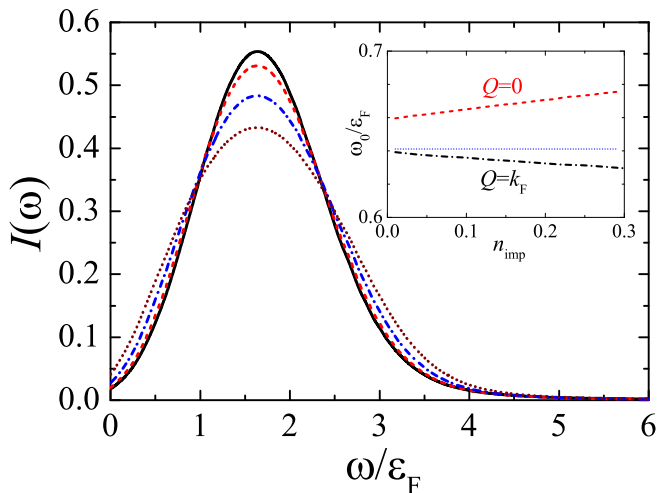


FIG. 4. The ejection Raman spectrum at different impurity densities: $n_{\text{imp}} = 0.01$ (black solid line), 0.05 (red dashed line), 0.15 (blue dot-dashed line), and 0.30 (brown dotted line), in units of the Fermi bath density n . Here, we consider the unitary limit at $T = 0.2T_F$. The transferred momentum is $Q = k_F$. The spectra are in units of ε_F^{-1} , and are normalized to unity (i.e., $\int d\omega I(\omega) = 1$). The inset shows $\omega_0 = \omega_{\text{peak}} - \hbar^2 Q^2/(2m)$ for the radio-frequency spectrum (with $Q = 0$) and for the Raman spectrum (with $Q = k_F$). The blue dotted line is the anticipated polaron energy $\omega_0 = |\mathcal{E}_P|$.

Raman signal, if the frequency ω satisfies

$$\omega = \epsilon_{\mathbf{k}+\mathbf{Q}}^{(I)} - \frac{\hbar^2 k^2}{2m^*} - \mathcal{E}_P \simeq \frac{\hbar^2 Q^2}{2m} - \mathcal{E}_P + \frac{\hbar^2 \mathbf{k} \cdot \mathbf{Q}}{m}. \quad (9)$$

After performing the integration over the angle between \mathbf{k} and \mathbf{Q} , the coherent contribution is therefore centered around the peak position, $\omega_{\text{peak}} \simeq \hbar^2 Q^2/(2m) - \mathcal{E}_P$. In Fig. 3, we examine the dependence of the Raman peak on the transferred momentum Q at two characteristic temperatures $T = 0.2T_F$ and $0.5T_F$ in the unitary limit. The peak position extracted from the Raman spectrum (solid circles) follows the anticipated trajectory $\hbar^2 Q^2/(2m) - \mathcal{E}_P$ (blue dotted lines), with the difference barely observable in the scale of the figure.

In Fig. 3, we also report the width of the Raman peak as a function of the transferred momentum Q (see red dashed lines). The width seems to be proportional to the transferred momentum at large Q . It is also strongly temperature dependent. Both the temperature dependence and linear Q -dependence might be understood from the last term in Eq. (9), since the width is directly related to the maximum value of Qk , which depends on both temperature and the impurity concentration. Therefore, from the width of Raman spectrum we can hardly extract useful information about the decay rate of Fermi polarons.

In contrast, as we discussed earlier, the peak position nicely follows the prediction $\omega_{\text{peak}} \simeq \hbar^2 Q^2/(2m) - \mathcal{E}_P$ and are not sensitive to both temperature (apart from the temperature-dependence in the polaron energy \mathcal{E}_P)

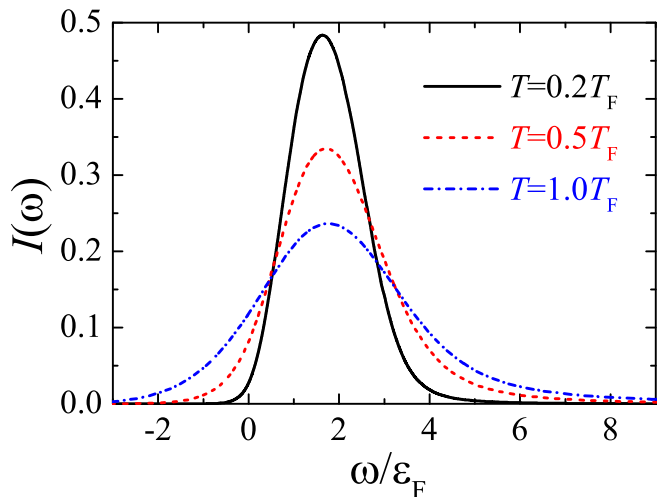


FIG. 5. The temperature dependence of the ejection Raman spectrum $I(\omega)$ [in units of ε_F^{-1}] at three temperatures: $T/T_F = 0.2$ (black solid line), 0.5 (red dashed line), and 1.0 (blue dot-dashed line). Here, we take a transferred momentum $Q = k_F$ and consider the unitary limit. The impurity concentration is $n_{\text{imp}}/n = 0.15$.

and the impurity concentration. Actually, the robustness of the peak position is one of the advantages of the Raman spectroscopy mentioned in the experimental work [13], owing to the significant change in momentum. In Fig. 4 we check specifically the dependence of the Raman spectrum on the impurity concentration n_{imp} . The spectrum becomes broader with increasing n_{imp} , while keeps its peak position nearly unchanged. In the inset, we subtract from ω_{peak} the background contribution $\hbar^2 Q^2/(2m)$ and define $\omega_0 = \omega_{\text{peak}} - \hbar^2 Q^2/(2m)$. We find that ω_0 shows a very weak red-shift with increasing impurity concentration at $Q = k_F$ (see the black dot-dashed line) and correctly approaches $|\mathcal{E}_P|$ in the single-impurity limit $n_{\text{imp}} \rightarrow 0$. This can be contrasted with the radio-frequency spectrum, where the peak position ω_0 fails to recover the anticipated value $|\mathcal{E}_P|$ and there is a small systematic shift at about $0.02\varepsilon_F$ in the single-impurity limit (i.e., the red dashed line). In Fig. 5, we also show the Raman spectrum at different temperatures in the unitary limit. The spectrum becomes broader with smaller peak height, as anticipated.

Finally, in Fig. 6 we report the ejection Raman spectrum in the strong coupling regime with $1/(k_F a) > 0$. Our non-self-consistent T -matrix theory becomes less accurate when we increase $1/(k_F a)$ at strong coupling [21, 23]. Nevertheless, we can see clearly that the spectrum becomes more and more asymmetric with increasing $1/(k_F a)$. This is because the coherent contribution from attractive polarons gets strongly suppressed. The incoherent part from the molecule-hole continuum in the impurity spectral function gives the major contribution to the Raman signal. It then features a highly asymmetric energy tail in the spectrum above the threshold

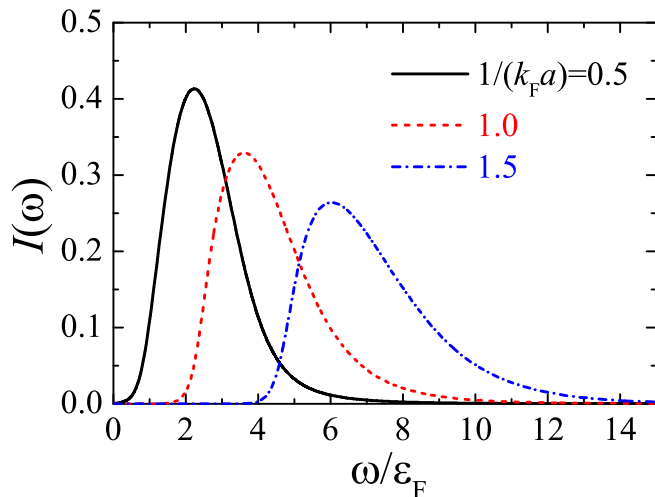


FIG. 6. The ejection Raman spectrum $I(\omega)$ [in units of ε_F^{-1}] below the Feshbach resonance at three interaction strengths: $1/(k_F a) = 0.5$ (black solid line), 1.0 (red dashed line), and 1.5 (blue dot-dashed line). We take a temperature $T = 0.2T_F$ and a transferred momentum $Q = k_F$. The impurity concentration is $n_{\text{imp}}/n = 0.15$.

$\omega_{\text{thres}} \simeq \hbar^2 Q^2 / (2m) + \mathcal{E}_B$, where \mathcal{E}_B is the binding energy of a molecule [13].

B. Injection Raman spectroscopy

We have so far discussed the ejection Raman spectroscopy, where the contribution from the high-energy part of the single-particle spectral function is thermally suppressed due to the Fermi distribution function in Eq. (6). As a result, the excited state of Fermi polarons, such as the repulsive polaron branch, can hardly be probed in the ejection scheme. This problem can be solved, if the impurity is initially prepared in a non-interacting state with the Fermi bath. The Raman beams can then bring the impurity into the interacting state, with a transfer rate as a function of the frequency recorded as the spectrum. In this *injection* scheme, the excited state of Fermi polarons can be directly observed [10]. By neglecting the initial-state effect, the injection Raman spectrum at the transferred momentum \mathbf{Q} is given by [28, 29],

$$I(\omega) = \frac{1}{V} \sum_{\mathbf{k}} A[\mathbf{k}, \epsilon_{\mathbf{k}+\mathbf{Q}}^{(I)} + \omega] f(\epsilon_{\mathbf{k}+\mathbf{Q}}^{(I)} - \mu_i), \quad (10)$$

where μ_i is the impurity chemical potential in the initial non-interacting state, to be determined by the number equation, $n_{\text{imp}} = (1/V) \sum_{\mathbf{k}} f(\epsilon_{\mathbf{k}}^{(I)} - \mu_i)$.

In Fig. 7, we show the injection Raman spectrum at the resonance (a) and at $1/(k_F a) = 0.5$ (b). Three typical Raman momenta are considered. In the unitary limit, for $Q \leq k_F$ we see clearly the bump structure at the energy $\omega \sim \varepsilon_F$, contributed from the precursor of the repulsive polaron. At $1/(k_F a) = 0.5$, the bumps develop

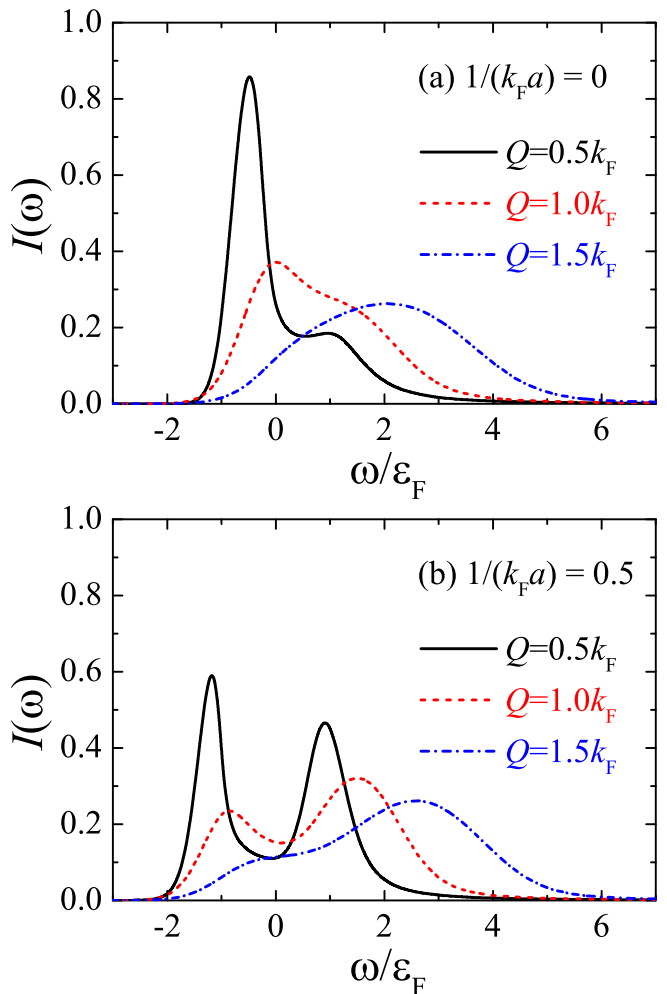


FIG. 7. The injection Raman spectrum $I(\omega)$ [in units of ε_F^{-1}] at the unitary limit $1/(k_F a) = 0.0$ (a) and at $1/(k_F a) = 0.5$ (b). We consider three different transferred momenta as indicated in the plots. The temperature is $T = 0.2T_F$ and the impurity concentration is $n_{\text{imp}}/n = 0.15$. The spectra are normalized to unity.

into well-defined repulsive polaron peaks. In this case, at $Q = 0.5k_F$ the widths of the low-energy attractive polaron peak and of the high-energy repulsive polaron peak are similar. Their weights (i.e., the integrated area under each peak) are also similar. However, as we increase the transferred momentum Q , the weight gradually transfers to the repulsive polaron peak. At large transferred momentum $Q = 1.5k_F$, the contributions from attractive and repulsive polaron basically merge into a very broad peak and somehow becomes featureless. Therefore, we suggest that an optimized transferred momentum $Q \sim k_F$ might be considered in the future experiments on the injection Raman spectroscopy.

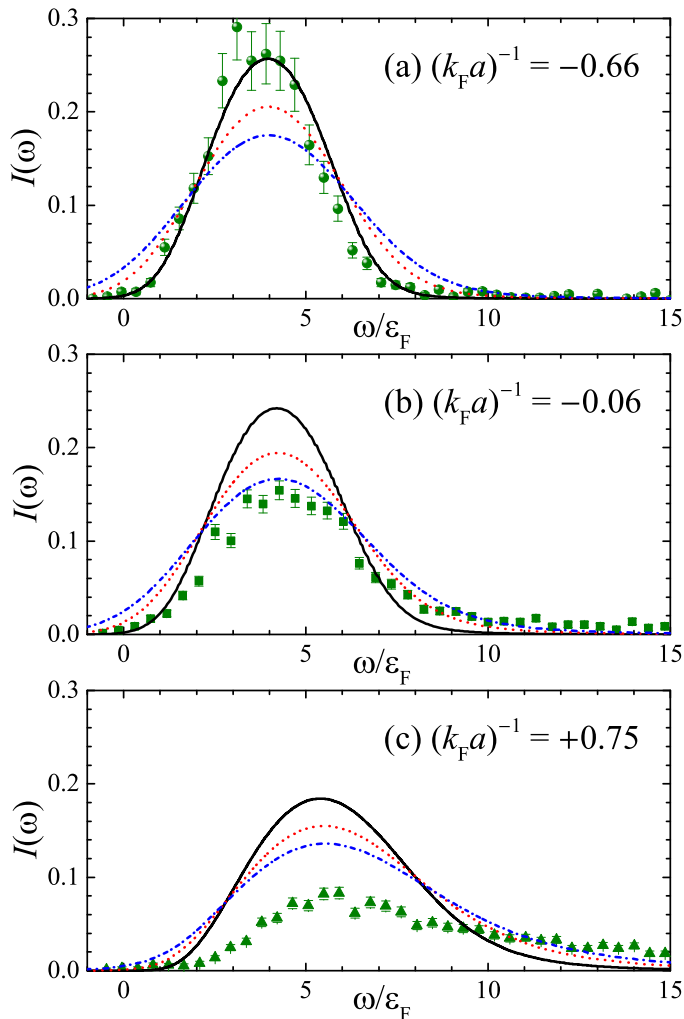


FIG. 8. The comparison of the theory (lines) with the experimental data from Ness *et al.* (symbols) [13], for the ejection Raman spectrum of a Fermi polaron across the Feshbach resonance. The spectra are in units of ε_F^{-1} and are normalized to unity, $\int d\omega I(\omega) = 1$. In the experiment, the temperature of the background Fermi gas is $T = 0.2T_F$ and the transferred momentum is $Q = 1.9k_F$. In our theoretical predictions, we consider three different temperatures: $T = 0.2T_F$ (black solid lines), $0.4T_F$ (red dashed lines) and $0.6T_F$ (blue dash-dotted lines). The impurity density is taken as $n_{\text{imp}}/n = 0.23$, following the experimental condition after an average over the trap configuration [13]. In the comparison, we do not include any adjustable free parameters.

C. Comparison with the experiment

We are now in the position to compare our theory with the recent experiment [13]. As shown in Fig. 8, we have considered three different temperatures for the theoretical curves ($0.2T_F$, $0.4T_F$, and $0.6T_F$, from the top to bottom), although experimentally the Fermi bath temperature is about $0.2T_F$. The other parameters such as the average impurity concentration $n_{\text{imp}} = 0.23n$ and the interaction strength $1/(k_F a)$ follow the experimental

condition [13], so there are no free adjustable parameters. The effect of spatial inhomogeneity caused by the external harmonic traps is considered in Appendix, which does not lead to qualitatively different results.

On the weak coupling side of the resonance (i.e., $1/(k_F a) = -0.66$ in Fig. 8(a)), we find a good agreement between the theoretical prediction and experimental data, both of which are given at the temperature $0.2T_F$. This agreement is anticipated, since our non-self-consistent T -matrix theory should work well with a weak impurity-bath interaction.

However, near the Feshbach resonance (i.e., the middle plot Fig. 8(b) for the case $1/(k_F a) = -0.06$), our low temperature prediction fails to explain the experimental data. A reasonable agreement for the peak height might be reached, if we increase the Fermi bath temperature to $0.6T_F$ in the theoretical calculation (see the blue dot-dashed line). This temperature is significantly higher than the experimental Fermi bath temperature. Tentatively, we attribute the disagreement between theory and experiment to the inefficiency of the non-self-consistent T -matrix theory for predicting the impurity spectral function, although we do know that the theory predicts very accurate polaron energy in the unitary limit at zero temperature [1, 17, 23]. On the other hand, it is worth mentioning that in the phenomenological theory used in the experiment [13], the temperature of the polaron T_P extracted from fitting is also systematically larger than the Fermi bath temperature ($0.2T_F$). Moreover, a large background temperature $T_{\text{bg}} = 2T_F$ is used for the incoherent contribution from molecules. The larger polaron temperature T_P and background temperature T_{bg} seem to be consistent with our finding that a larger Fermi bath temperature is theoretically needed to account for the experimental data.

At the strong coupling with $1/(k_F a) = 0.75$ in Fig. 8(c), our non-self-consistent T -matrix theory is completely unable to understand the experimental data. The data are about two times smaller than our theoretical result at $0.2T_F$. The peak position read from the data also seems to be larger than the theoretical prediction (i.e., $\omega_{\text{peak}} \simeq \hbar^2 Q^2 / (2m) - \mathcal{E}_P$), which we believe is reasonably accurate, since at zero temperature the T -matrix theory predicts a polaron energy \mathcal{E}_P that is in good agreement with quantum Monte Carlo simulation [1]. We note that, the disagreement between theory and experiment at strong coupling can hardly be reconciled by simply increasing the Fermi bath temperature in the theoretical calculation. Our theoretical prediction at $T = 0.6T_F$ shown in the blue dot-dashed line is still far above the experimental data.

IV. CONCLUSIONS AND OUTLOOKS

In summary, we have presented a microscopic calculation of Raman spectroscopy of Fermi polarons at finite temperature, based on a well-documented non-self-

consistent many-body T -matrix theory [1, 21, 23]. The dependences of the ejection Raman spectrum on the transferred Raman momentum, temperature, impurity concentration, and the impurity-bath interaction are systematically investigated. We have also considered the injection Raman spectrum, which might be experimentally measured in the near future.

We have compared our theoretical result with the recent ejection Raman spectroscopy measurement [13]. We have found a good agreement in the weak coupling regime, which is encouraging and anticipated. However, towards the Feshbach resonance and the strong coupling regime, the non-self-consistent T -matrix theory cannot provide a quantitative account of the experimental data. On the theoretical side, more refined treatments are therefore needed. By extending the existing zero temperature studies to the finite temperature case, the possible theoretical scenarios could include the functional renormalization group [26] and the diagrammatic quantum Monte Carlo simulation [17, 27].

ACKNOWLEDGMENTS

We thank Yoav Sagi and Richard Schmidt for fruitful discussions and for sharing the experimental data with us. This research was supported by the Australian Research Council's (ARC) Discovery Program, Grant No. DP180102018 (X.-J.L).

Appendix A: Raman spectrum within the local density approximation

In this Appendix, we consider the effect of spatial inhomogeneity on the Raman spectrum, caused by the external harmonic traps. We assume that the local density approximation (LDA) is applicable for the dynamical quantities such as the Raman spectroscopy. As the ejection Raman spectrum measures the transfer rate *per impurity*, the trap-averaged Raman spectrum takes the form [13],

$$\langle I(\omega) \rangle = \frac{\int d\mathbf{r} I(\omega, \mathbf{r}) n_I(\mathbf{r})}{\int d\mathbf{r} n_I(\mathbf{r})}, \quad (\text{A1})$$

where $n_I(\mathbf{r})$ is the impurity density distribution and $I(\omega, \mathbf{r})$ is the ejection spectrum calculated at the local position \mathbf{r} with local majority fermion density $n(\mathbf{r})$.

In general, the impurity distribution $n_I(\mathbf{r})$ is difficult to obtain, due to the interaction with majority fermions that leads to an (unknown) effective trapping potential. Here, since we are only interested in a *qualitative* estimate of the trapping effect, we may assume a fixed ratio between the local impurity density to the local majority fermion density, i.e., $n_I(r)/n(r) = n_{\text{imp}}/n = 0.23$. This assumption is reasonable, as the ejection Raman spectrum seems to depend weakly on n_{imp}/n , as shown in Fig. 4. Therefore, we replace in Eq. (A1) $n_I(\mathbf{r})$ by $n(\mathbf{r})$.

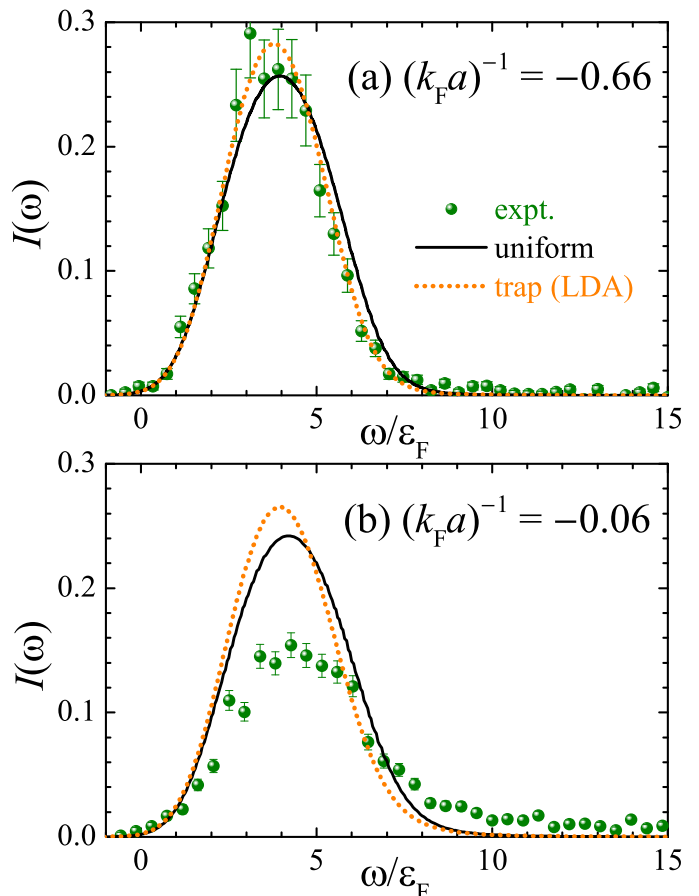


FIG. 9. The comparison of the theory (lines) with the experimental data from Ness *et al.* (symbols) [13] at the temperature $T = 0.2T_F$ and transferred momentum $Q = 1.9k_F$, for the ejection Raman spectrum of a Fermi polaron on the BCS side (a) and near the unitary limit (b). Here, $T_F = \varepsilon_F/k_B$ and k_F are the peak Fermi temperature and Fermi wavevector of majority fermions at the trap center, respectively. The spectra are in units of ε_F^{-1} and are normalized to unity, $\int d\omega I(\omega) = 1$. We present two theoretical predictions, for a uniform gas (black solid line) and a trapped gas (orange dotted line), calculated without and with the local density approximation, respectively. The local impurity density is always $n_{\text{imp}}/n = 0.23$.

The theoretical trap-averaged ejection Raman spectra at $1/(k_F a) = -0.66$ and $1/(k_F a) = -0.06$ are shown in Fig. 9, in the form of the orange dotted lines. As expected, the trap-average does not show a qualitative difference, in comparison with the theoretical predictions for a uniform gas, which have been discussed in detail in the main text. However, for the interaction parameter $1/(k_F a) = -0.66$ in Fig. 9(a), the trap-average does lead to a better agreement between theory and experiment, particularly at large frequency (i.e., $\omega > 5\varepsilon_F$). The disagreement between theory and experiment found near the unitary limit or on the strong-coupling BEC side can not be resolved by taking the trap-average.

-
- [1] P. Massignan, M. Zaccanti, and G. M. Bruun, Polarons, dressed molecules and itinerant ferromagnetism in ultracold Fermi gases, *Rep. Prog. Phys.* **77**, 034401 (2014).
- [2] Z. Lan and C. Lobo, A single impurity in an ideal atomic Fermi gas: current understanding and some open problems, *J. Indian Inst. Sci.* **94**, 179 (2014).
- [3] R. Schmidt, M. Knap, D. A. Ivanov, J.-S. You, M. Cetina, and E. Demler, Universal many-body response of heavy impurities coupled to a Fermi sea: a review of recent progress, *Rep. Prog. Phys.* **81**, 024401 (2018).
- [4] J. Wang, Functional Determinant Approach Investigations of Heavy Impurity Physics, arXiv:2011.01765 (2022).
- [5] C. Chin, R. Grimm, P. Julienne, and E. Tiesinga, Feshbach resonances in ultracold gases, *Rev. Mod. Phys.* **82**, 1225 (2010).
- [6] A. Schirotzek, C.-H. Wu, A. Sommer, and M.W. Zwierlein, Observation of Fermi Polarons in a Tunable Fermi Liquid of Ultracold Atoms, *Phys. Rev. Lett.* **102**, 230402 (2009).
- [7] Y. Zhang, W. Ong, I. Arakelyan, and J. E. Thomas, Polaron-to-Polaron Transitions in the Radio-Frequency Spectrum of a Quasi-Two-Dimensional Fermi Gas, *Phys. Rev. Lett.* **108**, 235302 (2012).
- [8] C. Kohstall, M. Zaccanti, M. Jag, A. Trenkwalder, P. Massignan, G.M. Bruun, F. Schreck, and R. Grimm, Metastability and coherence of repulsive polarons in a strongly interacting Fermi mixture, *Nature (London)* **485**, 615 (2012).
- [9] M. Koschorreck, D. Pertot, E. Vogt, B. Fröhlich, M. Feld, and M. Köhl, Attractive and repulsive Fermi polarons in two dimensions, *Nature (London)* **485**, 619 (2012).
- [10] F. Scazza, G. Valtolina, P. Massignan, A. Recati, A. Amico, A. Burchianti, C. Fort, M. Inguscio, M. Zaccanti, and G. Roati, Repulsive Fermi Polarons in a Resonant Mixture of Ultracold ^6Li Atoms, *Phys. Rev. Lett.* **118**, 083602 (2017).
- [11] Z. Yan, P. B. Patel, B. Mukherjee, R. J. Fletcher, J. Struck, and M.W. Zwierlein, Boiling a Unitary Fermi Liquid, *Phys. Rev. Lett.* **122**, 093401 (2019).
- [12] M. Cetina, M. Jag, R. S. Lous, I. Fritsche, J. T. M. Walraven, R. Grimm, J. Levinsen, M. M. Parish, R. Schmidt, M. Knap, and E. Demler, Ultrafast many-body interferometry of impurities coupled to a Fermi sea, *Science* **354**, 96 (2016).
- [13] G. Ness, C. Shkedorov, Y. Florshaim, O. K. Diessel, J. von Milczewski, R. Schmidt, and Y. Sagi, Observation of a Smooth Polaron-Molecule Transition in a Degenerate Fermi Gas, *Phys. Rev. X* **10**, 041019 (2020).
- [14] J. Wang, X.-J. Liu, and H. Hu, Exact Quasiparticle Properties of a Heavy Polaron in BCS Fermi Superfluids, *Phys. Rev. Lett.* **128**, 175301 (2022).
- [15] J. Wang, X.-J. Liu, and H. Hu, Heavy polarons in ultracold atomic Fermi superfluids at the BEC-BCS crossover: Formalism and applications, *Phys. Rev. A* **105**, 043320 (2022).
- [16] P. Massignan and G. M. Bruun, Repulsive polarons and itinerant ferromagnetism in strongly polarized Fermi gases, *Eur. Phys. J. D* **65**, 83 (2011).
- [17] N. Prokof'ev and B. Svistunov, Fermi-polaron problem: Diagrammatic Monte Carlo method for divergent sign-alternating series, *Phys. Rev. B* **77**, 020408(R) (2008).
- [18] M. Punk, P. T. Dumitrescu, and W. Zwerger, Polaron-to-molecule transition in a strongly imbalanced Fermi gas, *Phys. Rev. A* **80**, 053605 (2009).
- [19] R. Combescot, S. Giraud, and X. Leyronas, Analytical theory of the dressed bound state in highly polarized Fermi gases, *Europhys. Lett.* **88**, 60007 (2009).
- [20] F. Chevy, Universal phase diagram of a strongly interacting Fermi gas with unbalanced spin populations, *Phys. Rev. A* **74**, 063628 (2006).
- [21] H. Hu and X.-J. Liu, Fermi polarons at finite temperature: Spectral function and rf-spectroscopy, *Phys. Rev. A* **105**, 043303 (2022).
- [22] H. Hu, J. Wang, J. Zhou, and X.-J. Liu, Crossover polarons in a strongly interacting Fermi superfluid, *Phys. Rev. A* **105**, 023317 (2022).
- [23] R. Combescot, A. Recati, C. Lobo, and F. Chevy, Normal State of Highly Polarized Fermi Gases: Simple Many-Body Approaches, *Phys. Rev. Lett.* **98**, 180402 (2007).
- [24] H. Hu, B. C. Mulkerin, J. Wang, and X.-J. Liu, Attractive Fermi polarons at nonzero temperatures with a finite impurity concentration, *Phys. Rev. A* **98**, 013626 (2018).
- [25] B. C. Mulkerin, X.-J. Liu, and H. Hu, Breakdown of the Fermi polaron description near Fermi degeneracy at unitarity, *Ann. Phys. (NY)* **407**, 29 (2019).
- [26] R. Schmidt and T. Enss, Excitation spectra and rf response near the polaron-to-molecule transition from the functional renormalization group, *Phys. Rev. A* **83**, 063620 (2011).
- [27] O. Goulko, A. S. Mishchenko, N. Prokof'ev, and B. Svistunov, Dark continuum in the spectral function of the resonant Fermi polaron, *Phys. Rev. A* **94**, 051605(R) (2016).
- [28] P. Törmä, Spectroscopies—Theory, in *Quantum Gas Experiments* (World Scientific, Singapore, 2014). Chap. 10, pp. 199–250.
- [29] M. M. Parish, H. S. Adlong, W. E. Liu, and J. Levinsen, Thermodynamic signatures of the polaron-molecule transition in a Fermi gas, *Phys. Rev. A* **103**, 023312 (2021).